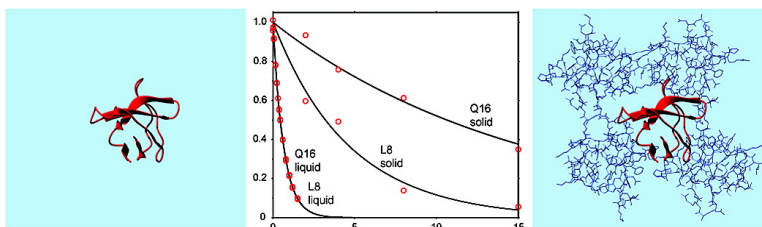


## Combined Analysis of N Relaxation Data from Solid- and Solution-State NMR Spectroscopy

Veniamin Chevelkov, Anastasia V. Zhuravleva, Yi Xue, Bernd Reif, and Nikolai R. Skrynnikov

*J. Am. Chem. Soc.*, **2007**, 129 (42), 12594-12595 • DOI: 10.1021/ja073234s • Publication Date (Web): 29 September 2007

Downloaded from <http://pubs.acs.org> on February 14, 2009



### More About This Article

Additional resources and features associated with this article are available within the HTML version:

- Supporting Information
- Links to the 7 articles that cite this article, as of the time of this article download
- Access to high resolution figures
- Links to articles and content related to this article
- Copyright permission to reproduce figures and/or text from this article

[View the Full Text HTML](#)

## Combined Analysis of $^{15}\text{N}$ Relaxation Data from Solid- and Solution-State NMR Spectroscopy

Veniamin Chevelkov,<sup>†</sup> Anastasia V. Zhuravleva,<sup>‡</sup> Yi Xue,<sup>‡</sup> Bernd Reif,<sup>\*,†</sup> and Nikolai R. Skrynnikov<sup>\*,‡</sup>

Forschungsinstitut für Molekulare Pharmakologie (FMP), Robert-Rössle-Strasse 10, 13125 Berlin, Germany, and Department of Chemistry, Purdue University, 560 Oval Drive, West Lafayette, Indiana 47907-2084

Received May 7, 2007; E-mail: nikolai@purdue.edu; reif@fmp-berlin.de

Nanosecond time-scale backbone dynamics in proteins has been a subject of much interest. While these motions can be detected by solution  $^{15}\text{N}$  relaxation methods,<sup>1</sup> they tend to be masked by the overall protein tumbling. As pointed out by Chen et al., “sometimes nanosecond time scale motions with a corresponding squared order parameter as low as 0.9 can go undetected, even with good quality data available at two magnetic fields”.<sup>2</sup> The situation can be improved if relaxation data are augmented by residual dipolar couplings (RDCs).<sup>3</sup> This approach, however, is experimentally demanding and the interpretation is complicated by “structural noise”, lack of absolute reference, and possible coupling between internal dynamics and alignment.<sup>4</sup>

Solid-state methods, on the other hand, are well-suited to detect nanosecond motions. In the absence of overall tumbling, slower forms of internal dynamics provide the most efficient channel of spin relaxation. However, because of experimental limitations it has been difficult to obtain a definitive picture of protein dynamics from the solid-state data alone. For instance, a wide range of effective correlation times, from hundreds of picoseconds to hundreds of nanoseconds, have been reported in the solid-state studies of proteins.<sup>5</sup>

In this Communication we undertake a *combined analysis of the solid- and solution-state relaxation data* from a small globular protein,  $\alpha$ -spectrin SH3 domain (spc SH3). It is common knowledge that structures of globular proteins as determined in solids and in solution are essentially identical. In fact, crystallographic structures provide the best models for analyzing solution NMR data.<sup>6</sup> Crystal contacts, which involve fluidlike layers formed by outward-pointing side chains,<sup>7</sup> have only limited impact. Taking this notion a step further, we suggest that internal protein dynamics in solids and in solution are also similar (assuming that the solid sample is well hydrated and the measurements are conducted at the same temperature). It is implied that the ‘soft’ interaction with environment does not alter native protein dynamics (note that the same assumption is made in the RDC-based studies of protein dynamics).

The combined analysis uses  $^{15}\text{N}$   $R_1$ ,  $R_2$ , and NOE data (500, 600 MHz) measured in solution, as well as  $^{15}\text{N}$   $R_1$  rates (600, 900 MHz) measured in solid (see Figure 1). The solution data were recorded using well-established experiments;<sup>8</sup> the solid-state data were obtained using an HSQC-style sequence (Figure S1, Supporting Information (SI)) applied to the deuterated sample with a 10% content of amide protons.<sup>9</sup> In the latter case, deuteration allows for  $^1\text{H}$  detection at high resolution, alleviates problems arising from proton-driven spin diffusion,<sup>10</sup> and avoids extensive probe heating caused by proton decoupling.

As a first step toward data interpretation, the solution data at two fields were analyzed by means of the  $R_2/R_1$  approach<sup>11</sup> yielding

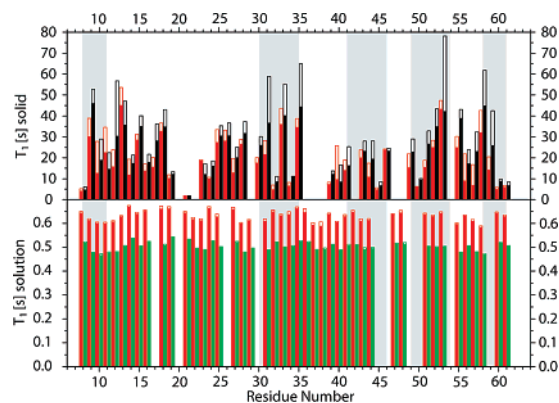


**Figure 1.**  $^{15}\text{N}$  solid- and solution-state  $T_1$  in spc SH3 as measured at 500, 600, and 900 MHz (green, red, and black bars, respectively). The empty portion of each bar corresponds to the experimental uncertainty. Shaded areas in the background indicate  $\beta$ -sheet structure. Sample conditions are listed in Table S1.

the diffusion parameters  $\tau_R^{\text{iso}} = 7.55$  ns (7 °C) and  $D_{\parallel}/D_{\perp} = 1.22$ . Consequently, the rotational anisotropy was modeled via the effective correlation times,  $\tau_R^{\text{eff}}$ , assigned to individual NH vectors and to the principal axes of  $^{15}\text{N}$  CSA tensors.<sup>12</sup> These  $\tau_R^{\text{eff}}$  values were used as the input for standard Lipari–Szabo analysis<sup>13</sup> (definitions of spectral densities are given in Table S2). The interpretation was (predictably) successful, with the experimental solution-state rates reproduced, on average, to within  $\pm 1.5\%$ .

The fast-motion parameters  $S_r^2$  and  $\tau_f$  determined from solution data analysis were subsequently used to predict the solid-state relaxation rates. In doing so, we assumed that fast local dynamics in solids and solution is identical and that it is the only source of relaxation in solids. Accordingly, the spectral densities of the form  $J(\omega) = (1 - S_r^2)\tau_f/(1 + \omega^2\tau_f^2)$  were used to calculate solid-state rates. As it turned out, the predicted solid-state  $R_1$  rates were significantly underestimated: on average, they amounted to 0.47 and 0.68 of the experimental rates (600 and 900 MHz, respectively). The discrepancy points toward the presence of additional motional modes that remain undetected in solution. Furthermore, the fact that better agreement is obtained for 900 MHz data suggests that these motions occur on the nanosecond time scale.<sup>14</sup>

In attempt to capture these motions, all data (six solution and two solid rates per residue) were analyzed jointly using the extended Clore–Lipari–Szabo model<sup>1</sup> parametrized with  $S_s^2$ ,  $\tau_s$ ,  $S_r^2$ , and  $\tau_f$ . In calculating solution rates,  $\tau_R^{\text{iso}}$  was treated as a global variable and adjusted to 7.75 ns. The tumbling anisotropy was accounted for as described above. In calculating solid rates, the contributions from overall tumbling were omitted (Table S2). Following careful optimization, the solution rates were fitted on average to within  $\pm 2.2\%$  and the solid rates to within  $\pm 3.6\%$ . The outcome of the fitting is illustrated in Figure S2.

<sup>†</sup> Forschungsinstitut für Molekulare Pharmakologie.

<sup>‡</sup> Purdue University.

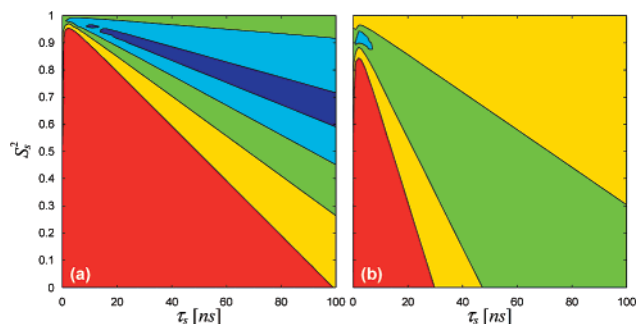


**Figure 2.**  $\chi$  surfaces for data from Gln-16 (a) and Leu-8 (b) interpreted by means of the Clore–Lipari–Szabo model.  $\chi = \langle |(\Gamma_i^{\text{fit}} - \Gamma_i^{\text{expt}})/\Gamma_i^{\text{expt}}| \rangle$ , where  $\Gamma_i$  denotes the complete set of relaxation data,  $i = 1-8$ , for a given residue. The map is generated by a grid search on  $S_s^2$ ,  $\tau_s$  plane, followed by simplex optimization relative to  $S_s^2$ ,  $\tau_s$  at each point of the grid. The magnitude of  $\chi$  is color-coded as follows: <2% (blue), 2–5% (cyan), 5–10% (green), 10–20% (yellow), >20% (red).

It can be readily recognized that the above procedure results in overfitting: indeed, solid-state rates are reproduced far better than can be expected based on the low precision of the measurements (Figure 1). Furthermore, the obtained solutions are not unique. Figure 2a illustrates the typical  $\chi$  surface in the coordinates  $S_s^2$ ,  $\tau_s$ . The long “valley” appearing in the plot demonstrates that the analysis effectively determines the ratio  $(1 - S_s^2)/\tau_s$  and fails to separate the two parameters. This is to be expected when solid-state data are limited to  $R_1$  rates and  $\tau_s$  falls in the macromolecular limit,  $\tau_s > \sim 10$  ns. Similar behavior has been observed in the pioneering study of Giraud et al.<sup>5d</sup>

The above treatment shows that solid- and solution-state data can be interpreted jointly using the same set of dynamic parameters. To validate this result, we prepared three additional samples of spc SH3 containing 20%, 30%, and 40% w/w of glycerol (see SI for details). Protein molecules in a water–glycerol mixture tend to be surrounded by water<sup>15</sup> and thus retain natively internal dynamics. The overall tumbling, however, is slowed down ( $t_R^{150}$  is 11.0, 13.8, and 17.4 ns, respectively), so that slow local motions play a more prominent role in spin–lattice relaxation.<sup>16</sup> As it turns out,  $R_1$ ,  $R_2$ , and NOE data from the three water–glycerol samples can be successfully included in the solid and solution fitting procedure. The result is a credible picture of internal dynamics in the spc SH3. For example, when the optimization is restricted to a (physically reasonable) region  $S_s^2 > 0.8$ , the solution-state relaxation parameters are reproduced, on average, to within 3.2% and the solid-state rates to within 5.4%. For half of the analyzed residues (17 out of 35) the amplitude of the slow motion turns out to be very small,  $S_s^2 > 0.97$  (furthermore, for all but three residues  $S_s^2 > 0.92$ ). The respective correlation times  $\tau_s$  fall in the interval from 0.8 to 54 ns (average 11.5 ns). The fast-motion order parameters  $S_f^2$  range from 0.77 to 0.90 (average 0.83) and  $\tau_f$  from 0 to 39 ps (average 14 ps). Note, however, that separation of  $S_s^2$  and  $\tau_s$  remains tentative even with the addition of the new data.

For further corroboration of the method we turned to the MD simulations. A 30-ns trajectory of spc SH3 in explicit solvent was generated using CHARMM equipped with the CMAP module.<sup>17</sup> The correlation functions were extracted in a standard fashion (with the overall tumbling subtracted out)<sup>18</sup> and used to predict the solid-state  $^{15}\text{N}$   $R_1$  rates. While the agreement on a per-residue basis was poor, roughly one-half of the simulated rates turned out to be overestimated and another half underestimated (Figure S3). Thus,

small-amplitude ns motions observed in solution simulation can, in principle, account for the relaxation rates measured in solid.

Several conclusions can be reached on the basis of the presented results. (i) Fast (ps) motions are responsible for a significant portion of backbone  $R_1$  rates in solids, while the remainder comes from ns dynamics. (ii) Small-amplitude ns motions observed in solids are likely to be present also in solution. (iii) The combined analysis of solid- and solution-state relaxation data offers a promising tool for detailed characterization of ps–ns motions in the protein backbone. Such combined analysis can be strengthened by the addition of new solid-state relaxation experiments. In particular, if the data set is complemented with solid  $R_2$ -type data (e.g., transverse cross-correlations<sup>19</sup>) the reliable separation of  $S_s^2$  and  $\tau_s$  can be effected. It is expected that the proposed approach will provide new and stimulating insights into protein dynamics.

**Acknowledgment.** We are grateful to Flemming Hansen and Lewis Kay for help with 500 MHz measurements and to the anonymous reviewer for suggesting water–glycerol experiments.

**Supporting Information Available:** Solid-state pulse sequence for measuring  $^{15}\text{N}$   $R_1$  relaxation; table of solid- and solution-state relaxation rates; expressions for spectral densities; figure illustrating data fitting with Clore–Lipari–Szabo model; comparison of the experimental and MD-simulated  $R_1$  rates in solids; comparison of the experimental and predicted  $R_1$  rates in the water–glycerol solution; table of  $S_s^2$ ,  $\tau_s$ ,  $S_f^2$ , and  $\tau_f$ . This material is available free of charge via the Internet at <http://pubs.acs.org>.

## References

- (1) Clore, G. M.; Szabo, A.; Bax, A.; Kay, L. E.; Driscoll, P. C.; Gronenborn, A. M. *J. Am. Chem. Soc.* **1990**, *112*, 4989–4991.
- (2) Chen, J. H.; Brooks, C. L.; Wright, P. E. *J. Biomol. NMR* **2004**, *29*, 243–257.
- (3) (a) Lakomek, N. A.; Farès, C.; Becker, S.; Carlomagno, T.; Meiler, J.; Griesinger, C. *Angew. Chem., Int. Ed.* **2005**, *44*, 7776–7778. (b) Bouvignies, G.; Bernado, P.; Meier, S.; Cho, K.; Grzesiek, S.; Brüschweiler, R.; Blackledge, M. *Proc. Natl. Acad. Sci. U.S.A.* **2005**, *102*, 13885–13890.
- (4) (a) Zweckstetter, M.; Bax, A. *J. Biomol. NMR* **2002**, *23*, 127–137. (b) Clore, G. M.; Schwieters, C. D. *J. Am. Chem. Soc.* **2004**, *126*, 2923–2938.
- (5) (a) Cole, H. B. R.; Torchia, D. A. *Chem. Phys.* **1991**, *158*, 271–281. (b) North, C. L.; Cross, T. A. *Biochemistry* **1995**, *34*, 5883–5895. (c) Mack, J. W.; Usha, M. G.; Long, J.; Griffin, R. G.; Wittebort, R. J. *Biopolymers* **2000**, *53*, 9–18. (d) Giraud, N.; Blackledge, M.; Goldman, M.; Böckmann, A.; Lesage, A.; Penin, F.; Emsley, L. *J. Am. Chem. Soc.* **2005**, *127*, 18190–18210.
- (6) Bax, A. *Protein Sci.* **2003**, *12*, 1–16.
- (7) Zhou, Y. Q.; Vitkup, D.; Karplus, M. *J. Mol. Biol.* **1999**, *285*, 1371–1375.
- (8) Farrow, N. A.; Muhandiram, R.; Singer, A. U.; Pascal, S. M.; Kay, C. M.; Gish, G.; Shoelson, S. E.; Pawson, T.; Forman-Kay, J. D.; Kay, L. E. *Biochemistry* **1994**, *33*, 5984–6003.
- (9) Chevelkov, V.; Rehbein, K.; Diehl, A.; Reif, B. *Angew. Chem., Int. Ed.* **2006**, *45*, 3878–3881.
- (10) Giraud, N.; Blackledge, M.; Böckmann, A.; Emsley, L. *J. Magn. Reson.* **2007**, *184*, 51–61.
- (11) Tjandra, N.; Feller, S. E.; Pastor, R. W.; Bax, A. *J. Am. Chem. Soc.* **1995**, *117*, 12562–12566.
- (12) Lee, L. K.; Rance, M.; Chazin, W. J.; Palmer, A. G. *J. Biomol. NMR* **1997**, *9*, 287–298.
- (13) Lipari, G.; Szabo, A. *J. Am. Chem. Soc.* **1982**, *104*, 4546–4559.
- (14) The contribution from ns motions into  $R_1$  is reduced at the higher field.
- (15) Gekko, K.; Timasheff, S. N. *Biochemistry* **1981**, *20*, 4667–4676.
- (16) Korchuganov, D. S.; Gagnidze, I. E.; Tkach, E. N.; Schulga, A. A.; Kirpichnikov, M. P.; Arseniev, A. S. *J. Biomol. NMR* **2004**, *30*, 431–442.
- (17) Buck, M.; Bouguet-Bonnet, S.; Pastor, R. W.; MacKerell, A. D. *Biophys. J.* **2006**, *90*, L36–L38.
- (18) Chandrasekhar, I.; Clore, G. M.; Szabo, A.; Gronenborn, A. M.; Brooks, B. R. *J. Mol. Biol.* **1992**, *226*, 239–250.
- (19) (a) Chevelkov, V.; Faelber, K.; Schrey, A.; Rehbein, K.; Diehl, A.; Reif, B. *J. Am. Chem. Soc.* **2007**, *129*, 10195–10200. (b) Chevelkov, V.; Diehl, A.; Reif, B. *Magn. Reson. Chem.* In press, 2007. (c) Skrynnikov, N. R. *Magn. Reson. Chem.* In press, 2007.

JA073234S